

Search for CP Violating Signature of Intergalactic Magnetic Helicity in the Gamma Ray Sky

Hiroyuki Tashiro[†], Wenlei Chen^{*}, Francesc Ferrer^{*}, Tanmay Vachaspati[†]

[†]*Physics Department, Arizona State University, Tempe, Arizona 85287, USA.*

^{*}*Physics Department and McDonnell Center for the Space Sciences, Washington University, St. Louis, MO 63130, USA.*

11 September 2018

ABSTRACT

The existence of a cosmological magnetic field could be revealed by the effects of non-trivial helicity on large scales. We evaluate a CP odd statistic, Q , using gamma ray data obtained from Fermi satellite observations at high galactic latitudes to search for such a signature. Observed values of Q are found to be non-zero; the probability of a similar signal in Monte Carlo simulations is $\sim 0.2\%$. Contamination from the Milky Way does not seem to be responsible for the signal since it is present even for data at very high galactic latitudes. Assuming that the signal is indeed due to a helical cosmological magnetic field, our results indicate left-handed magnetic helicity and field strength $\sim 10^{-14}$ G on ~ 10 Mpc scales.

Parity (P) and charge conjugation (C) symmetry violating processes in the early universe, such as during matter-antimatter annihilation, may have produced a helical magnetic field, with important implications for the structures we observe. In this case, the observation of a cosmological magnetic field can probe the very early universe ($t \lesssim 1$ ns), provide information about particle physics at very high temperatures ($T \gtrsim 1$ TeV), and also characterize the cosmological environment prior to structure formation.

Several tools to detect and study a cosmological magnetic field are known, including Faraday rotation of distant polarized sources and the cosmic microwave background (CMB), and the distribution of GeV gamma rays from TeV blazars (see Durrer & Neronov (2013) for a recent review). However, there are very few ideas for how to directly measure the helicity of a magnetic field (Kahniashvili & Vachaspati 2006; Tashiro & Vachaspati 2013). The helicity of a magnetic field may be viewed as due to the screw-like (or linked) distribution of magnetic field lines. More formally, the magnetic helicity density within a large volume V is defined as

$$h = \frac{1}{V} \int_V d^3x \mathbf{A} \cdot \mathbf{B},$$

where \mathbf{A} is the electromagnetic potential of magnetic field, $\mathbf{B} = \nabla \times \mathbf{A}$. Magnetic helicity is odd under combined charge conjugation plus parity (CP) transformations.

Indirect measures of magnetic helicity rely on measuring the non-helical power spectrum and then deducing properties of the helical spectrum on the basis of MHD evolution (Christensson et al. 2005; Campanelli 2004; Banerjee & Jedamzik 2004; Campanelli 2007; Boyarsky et al. 2012; Kahniashvili et al. 2013), or else by constructing parity odd cross-correlators of CMB temperature and polarization (Caprini et al. 2004; Kahniashvili & Ratra 2005; Kunze 2012). Direct measures can only rely on the propagation of

charged particles through the magnetic field as these sample the full three dimensional distribution of the field. Thus cosmic rays are sensitive to magnetic helicity (Kahniashvili & Vachaspati 2006), as are GeV gamma rays that are produced due to cascades originating from TeV blazars (Tashiro & Vachaspati 2013). In the latter process, the original TeV photon produces an electron-positron pair by scattering with extragalactic background light (EBL) in a cosmological void region. The charged pair then propagate in the intervening magnetic field, and finally up-scatter CMB photons to produce GeV gamma rays. In the context of a single TeV source, observed GeV gamma rays then carry information about the helicity of the intervening magnetic field. A key point of the present paper, also alluded to in Tashiro & Vachaspati (2013), is that the observed *diffuse* gamma ray sky may also hold information about the cosmological helical magnetic field and CP violation in the early universe.

Assume we are located within the jet opening angle of a blazar but are off-axis (see Fig. 1). A photon of energy $E_1 \sim$ TeV from the blazar propagates a distance $D_{\text{TeV}1} \sim 100$ Mpc and then scatters with an EBL photon to produce an electron-positron pair (Neronov & Semikoz 2009). The electron (positron) bends in the cosmological magnetic field and, after a typical distance of about 30 kpc, up-scatters a CMB photon, that arrives to the observer at the vectorial position Θ_1 in the observation plane. Similarly, another photon of energy E_2 arrives at Θ_2 . Note that the line-of-sight to the source defines the origin on the observation plane.

Let us define $G(E_1, E_2) = \langle \Theta(E_1) \times \Theta(E_2) \cdot \hat{x} \rangle$, where \hat{x} is perpendicular to the plane of observation and points towards the source, and the ensemble average is over all observed photons from the blazar. In Tashiro & Vachaspati

arXiv:1310.4826v4 [astro-ph.CO] 11 Sep 2014

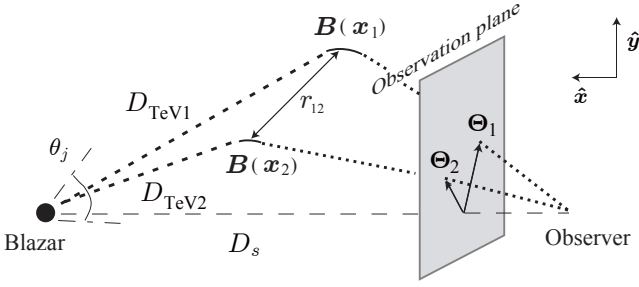


Figure 1. Events at two different energies sample the magnetic field in regions of size $D_e \sim 30$ kpc (solid lines at the vertices of the triangles). The regions themselves are separated by distance r which can be ~ 100 Mpc depending on the energy difference of the two events. (Figure taken from [Tashiro & Vachaspati 2013](#).)

(2013) it was shown that

$$G(E_1, E_2) \propto \frac{1}{2} M_H(|r_{12}|) r_{12}. \quad (1)$$

where M_H is the helical correlation function of the intervening magnetic field and defined by

$$\langle B_i(\mathbf{x} + \mathbf{r}) B_j(\mathbf{x}) \rangle = M_N(r) \left[\delta_{ij} - \frac{r_i r_j}{r^2} \right] + M_L(r) \frac{r_i r_j}{r^2} + M_H(r) \epsilon_{ijl} r^l. \quad (2)$$

The distance r_{12} in Eq. (1) is given in terms of the energies,

$$r_{12} \approx D_{\text{TeV}}(E_1) - D_{\text{TeV}}(E_2) \quad (3)$$

with

$$D_{\text{TeV}}(E_{\text{TeV}}) \sim 80 \frac{\kappa}{(1+z_s)^2} \text{Mpc} \left(\frac{E_{\text{TeV}}}{10 \text{ TeV}} \right)^{-1}, \quad (4)$$

where z_s is the redshift of the source and κ is a parameter that depends on the EBL. We will take $1+z_s \sim 1$ and $\kappa \sim 1$ ([Neronov & Semikoz 2009](#)). The overall proportionality factors in Eq.(1) depend on geometrical parameters such as the distance to the source and the energies, and will not be important for what follows. Note that r_{12} is positive if $E_1 < E_2$ because higher energy photons from the blazar produce electron-positron pairs more easily and so $D_{\text{TeV}}(E_1) > D_{\text{TeV}}(E_2)$.

The correlation $G(E_1, E_2)$ is defined only if the TeV blazar is visible, since the vectors Θ originate at the location where the line of sight intersects the observational plane. What if the TeV blazar is not visible? We can still measure the helicity of an intervening magnetic field by noting that the highest energy photons deviate the least from the source position. We can thus approximate the position of the blazar by the position of a photon with the highest energy E_3 and the relevant correlator is

$$G(E_1, E_2; E_3) = \langle (\Theta(E_1) - \Theta(E_3)) \times (\Theta(E_2) - \Theta(E_3)) \cdot \hat{\mathbf{x}}_3 \rangle$$

and we will always assume the ordering $E_1 < E_2 < E_3$. The vector $\hat{\mathbf{x}}_3$ points in the direction of the E_3 photon.

Diffuse gamma rays are observed on a sphere (the sky) and not on a plane and so the statistic $G(E_1, E_2; E_3)$ needs to be modified suitably. We propose the statistic (which is

almost our final expression),

$$\begin{aligned} Q'(E_1, E_2, E_3) &= \langle (\mathbf{n}(E_1) - \mathbf{n}(E_3)) \times \\ &\quad (\mathbf{n}(E_2) - \mathbf{n}(E_3)) \cdot \mathbf{n}(E_3) \rangle \\ &= \langle \mathbf{n}(E_1) \times \mathbf{n}(E_2) \cdot \mathbf{n}(E_3) \rangle, \end{aligned}$$

where $\mathbf{n}(E)$ denotes the (unit) vector to the location of the photon of energy E on the sky.

The problem with Q' is that we cannot be sure that the photon of energy E_3 corresponds reasonably to a source for cascade photons. Also, in the case when the TeV source was known, the ensemble average is taken over all cascade photons *originating from the source*. In our case, we don't even know if there is a TeV source, let alone which photons originate from a cascade and which do not. However, if we work on the hypothesis that some of the photons that are not too far away from the location of an E_3 photon originate from the same source and are possibly due to a cascade, the statistic should still make sense if we restrict the average to a region close to the location of the E_3 photon. (Note that such a region may contain photons unrelated to the E_3 cascade, but their contribution to the odd-statistic Q will add up to zero on average.) To do this we can introduce a window function that will preferably sample E_1 and E_2 photons close to the chosen E_3 photon. The simplest implementation, and the one we have chosen, is to use a top-hat window function with a radius that we treat as a free parameter. Further, we ensemble average over all E_3 photons since we do not know if any given E_3 photon is due to a TeV source. Then, our final expression for the statistic is

$$\begin{aligned} Q(E_1, E_2, E_3, R) &= \frac{1}{N_1 N_2 N_3} \times \\ &\quad \sum_{i=1}^{N_1} \sum_{j=1}^{N_2} \sum_{k=1}^{N_3} W_R(\mathbf{n}_i(E_1) \cdot \mathbf{n}_k(E_3)) W_R(\mathbf{n}_j(E_2) \cdot \mathbf{n}_k(E_3)) \\ &\quad \mathbf{n}_i(E_1) \times \mathbf{n}_j(E_2) \cdot \mathbf{n}_k(E_3), \end{aligned}$$

where the indices i, j, k refer to different photons and the top-hat window function W_R is given by

$$W_R(\cos \alpha) = \begin{cases} 1, & \text{for } \alpha \leq R \\ 0, & \text{otherwise.} \end{cases} \quad (5)$$

With a top-hat window function, the statistic can also be written as

$$Q(E_1, E_2, E_3, R) = \frac{1}{N_3} \sum_{k=1}^{N_3} \boldsymbol{\eta}_1 \times \boldsymbol{\eta}_2 \cdot \mathbf{n}_k(E_3) \quad (6)$$

where $\boldsymbol{\eta}_a = (1/N_a) \sum_{i \in D(\mathbf{n}_k, R)} \mathbf{n}_i(E_a)$, $a = 1, 2$ and $D(\mathbf{n}_k(E_3), R)$ is the ‘‘patch’’ in the sky with center at the location of $\mathbf{n}_k(E_3)$ and radius R degrees. Essentially, $\boldsymbol{\eta}_a$ are the average locations of photons of energy E_a within a patch, and Q is given by the radial component of $\boldsymbol{\eta}_1 \times \boldsymbol{\eta}_2$ averaged over all patches in the sky that are centered on photons with energy E_3 .

An intuitive picture for the meaning of the correlator is shown in Fig. 2. We observe photons of three different energies (illustrated by three different colors) on the cut-sky away from the galactic plane. We assume that the highest energy E_3 photons approximately represent the source directions. Lower energy (E_1 and E_2) photons in patches of some radius R around the position of the E_3 photon are more likely to be from the same source. Then we consider

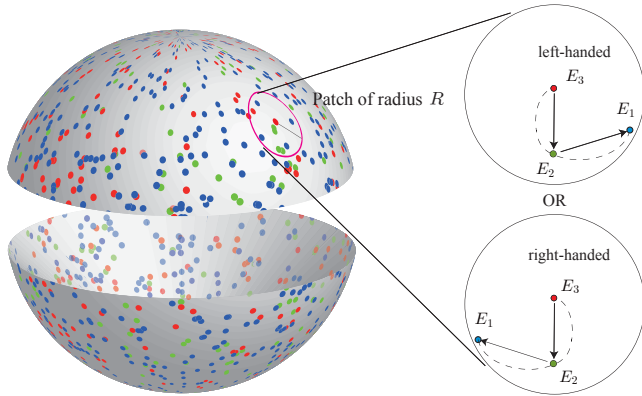


Figure 2. Illustration of the cut-sky with gamma rays distributed on it. Patches of radius R degrees are centered on the highest energy gamma rays. In those patches we test if the lower energy photons are distributed along left- or right-handed spirals.

the vectors in the patches as shown in Fig. 2 and ask if the directed curves from E_3 to E_2 to E_1 are bent to the left or to the right, *i.e.* are the photons of decreasing energy in patterns of left-handed or right-handed spirals? A positive (negative) value of the statistic Q implies that there is an excess of right-handed (left-handed) spirals in the gamma ray sky.

Next we measure the value of Q on the emission detected by the Fermi-LAT, using ~ 60 months of data.* The data were processed with the FERMI SCIENCE TOOLS† to mask regions of the sky heavily contaminated by Galactic diffuse emission and known point sources. We selected LAT data from early-August 2008 through end of January 2014 (weeks 9 to 307) that were observed at galactic latitudes, $|GLAT| \geq 50^\circ$. To ensure that the events are photons with high probability, we use the Pass 7 Reprocessed data in the CLEAN event class. Contamination from photons produced by cosmic-ray interactions in the upper atmosphere is avoided by excluding events with zenith angles greater than 100° , and only data for time periods when the spacecraft’s rocking angle was below 52° were considered. Since we are interested in the diffuse emission, we mask out a 3° angular diameter around each source in the First LAT High-Energy Catalog (The Fermi-LAT Collaboration, 2013).

We restrict our analysis to the energy range 10 – 60 GeV and we bin the data in 5 linearly spaced energy bins of width $\Delta E = 10$ GeV. We will label events with energies in $(E, E + \Delta E)$ by E , e.g. 10 GeV photons refers to data in the (10, 20) GeV bin. The total number of photons above 60° absolute galactic latitude in each of the five bins of increasing energy is 7053, 1625, 726, 338 and 200. We then evaluated Q using Eq. (6) for patches of radius $R = 1^\circ - 20^\circ$ and for each of the six possible combinations of $E_1 < E_2 < E_3 = 50$ GeV as shown in Fig. 3. The left and right columns display the analysis with $E_3 = 50$ GeV photons that are restricted to lie with absolute galactic latitude larger than 70° and 80° re-

spectively. For the smallest values of R , some of the patches centered on the highest energy E_3 events will not contain any low-energy photon, and we set $Q = 0$ in this case. To each data point we associate the “standard error” bar, which is given by the standard deviation of the distribution of Q values over different patches, σ_Q , divided by $\sqrt{N_3}$ where N_3 is the number of E_3 photons, which is the same as the number of patches. Thus, $\delta Q = \sigma_Q / \sqrt{N_3}$. We also evaluated errors due to the Fermi-LAT PSF‡. We added (Gaussian) noise to the data consistent with the PSF in every energy bin. As the width of the PSF in the lowest energy bin is ~ 8 arcmin, these resolution errors are small, of order 10% of the standard error, and are not shown. For comparison, we have generated synthetic data using a uniform distribution of gamma rays at each energy. Since we are only looking at the diffuse gamma ray background and have cut out identified sources, a uniform distribution is a reasonable model. The mean value of Q and its standard deviation are evaluated over 10^4 realizations of synthetic data that are treated exactly like the real data. As shown in Fig. 3, the mean value for the synthetic data is zero as no CP violation is present. The 1σ spread obtained from the synthetic data, and the standard error obtained from real data are comparable. To quote error bars we always take the larger of the two spreads.

Non-zero values of Q at greater than 2σ level occur for several energy combinations and for different patch sizes. Most significantly, the (10,40) energy combination plot in the right column shows $> 2\sigma$ deviations from zero for all patch sizes from $R = 8^\circ - 20^\circ$. We should keep in mind, however, that we have scanned over several parameters and the actual significance of our results should be modulated by a penalty factor discussed further below.

When we analyze the (10,40) data separately for the northern and southern hemispheres, as in Fig. 4, we find non-zero Q values with $\gtrsim 3\sigma$ significance in the northern hemisphere with $R = 11^\circ - 20^\circ$. The signal in the southern hemisphere is marginally below the 2σ level. One possible reason is that photon statistics in the south is 10-33% poorer in the four energy bins in the 10-50 GeV range. Another possible reason is that there genuinely is a north-south asymmetry in the cascade photons, especially in the small polar regions we are considering. As more data is collected, a clearer picture will emerge.

Our results have an interpretation in terms of cascade gamma rays originating from TeV blazars in the presence of a cosmological magnetic field with helicity. However there are other possibilities too. We now discuss that the signal may be due to contamination, or a statistical fluctuation, or perhaps a systematic error.

We have tested the possibility of Milky Way contamination by only considering patches centered at very high absolute galactic latitudes. We find that the signal actually grows stronger if we restrict the patch centers to be at higher absolute galactic latitudes ($|b| > 80^\circ$ compared to $|b| > 70^\circ$). The stronger signal at high latitudes suggests that the effect is extragalactic. In addition, if Milky Way contamination was responsible for the signal, the signal should continue to

* Our analysis tools are available on the wiki https://sites.physics.wustl.edu/magneticfields/wiki/index.php/Search_for_CP_violation_in_the_gamma_ray_sky.

† The Fermi Science Support Center (FSSC), <http://fermi.gsfc.nasa.gov/ssc>

‡ http://fermi.gsfc.nasa.gov/ssc/data/analysis/documentation/Cicerone/Cicerone_LAT_IRFs/IRF_PSF.html

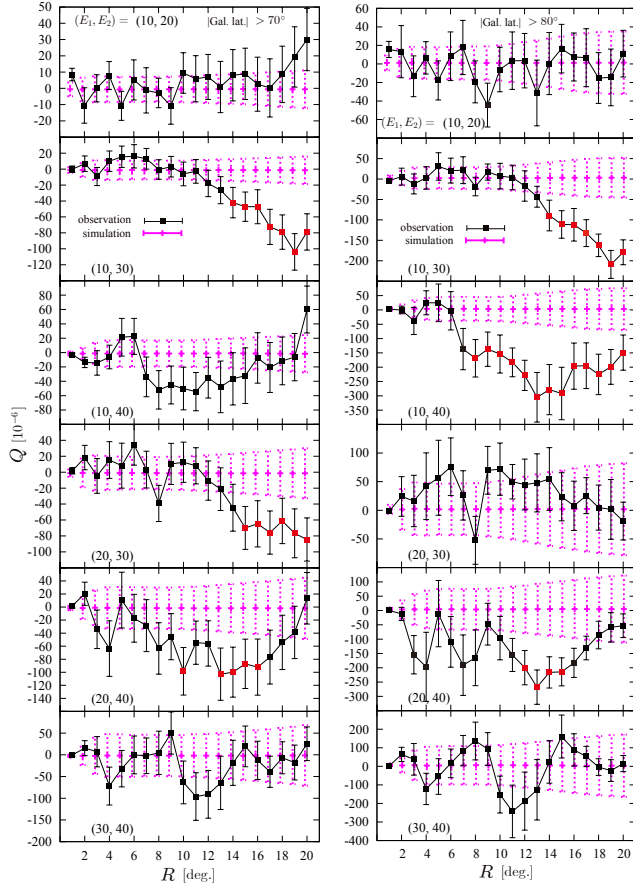


Figure 3. Q vs. patch radius in degrees for different combinations of $\{E_1, E_2\} \in \{10, 20, 30, 40\}$ GeV when patches centered on $E_3 = 50$ GeV photons are considered at absolute galactic latitude greater than 70° (left column) and 80° (right column). Also, shown are 1σ spreads (magenta error bars) obtained from simulated data. Q values that are non-zero at greater than 2σ are shown by red squares in the plots.

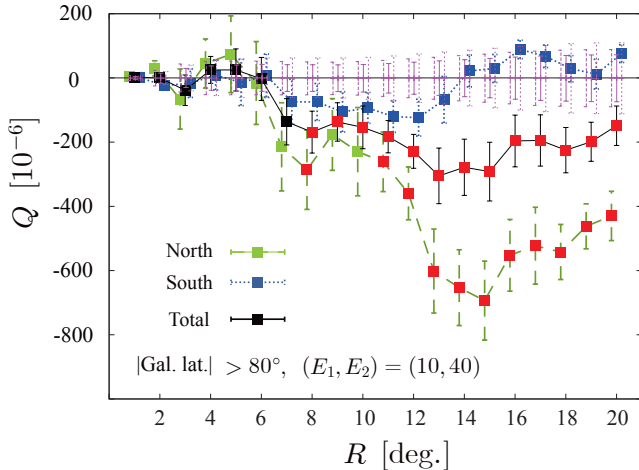


Figure 4. Q vs. R for the northern and southern hemispheres and for both combined. The southern hemisphere Q values are consistent with zero at the $\sim 2\sigma$ level; the northern hemisphere values are non-zero even at the $\sim 3\sigma$ level for larger patches.

grow for large R since such patches extend to lower galactic latitudes. However, we see a peak structure at $R \sim 12^\circ$.

As alluded to above, scanning over several parameters might artificially bias the significance of the signal. To account for this so called “look elsewhere effect” we estimate the “penalty factor” introduced by our scanning over angle and energy. We perform a Monte Carlo simulation, in which synthetic data is subject to the same analysis as the real dataset, and count the occurrence of Q values that deviate by more than 2σ for 13 consecutive values of patch radii, R , in *any* energy bin, (E_1, E_2) , and with cuts of $|b| > 70^\circ, 80^\circ$. Such signals only appear with probability ~ 0.002 . As more data is accumulated, our findings will become more robust as we will have smaller error bars. In addition, since the signal should also appear in future data, we will be able to confirm our positive findings at patch radius $\Theta \approx 12^\circ$ without the need for scanning over parameters.

Systematic errors may be present in the data sets we have used for some unknown experimental reasons. These are difficult to track down but it makes sense to ask what systematic transformations of the data might eliminate the signal. Since Q is a (pseudo) scalar, it is unaffected by an overall rotation. If we could rotate only photons in one energy bin and in each individual patch around the axis through the center of the patch, we may be able to undo the signal. However, such a rotation on the data is not possible because there are many overlapping patches on the sky and the rotation cannot be defined for photons in the regions common to two distinct patches. A systematic transformation we have investigated is a rotation of the 10 – 20 GeV photons about the polar axis, and in opposite senses in the northern and southern hemispheres. The transformation shifts the azimuthal angles of only the 10 GeV bin by an angle α in the northern hemisphere, and by $-\alpha$ in the southern hemisphere, where α is varied in steps of 10 arcminutes in the interval $(-0.5^\circ, +0.5^\circ)$. However, we find that the value of Q remains unchanged by these rotations. If the signal is due to some other systematic, these need to be quite complicated as the photons at different energies need to be shifted with respect to each other in a parity odd way, and in such a way that the signal does not re-appear in the energy combinations where it is currently absent. In a preliminary analysis, we have used the Fermi time exposure data to perform Monte Carlo simulations and still find the signal to be significant. We are currently exploring other tests.

Next we assume that the signal is indeed due to the cascade process in the presence of a cosmological magnetic field. What properties of the magnetic field can we deduce from the results?

We can estimate the magnetic field strength if we assume that the patch radius at which we get a signal is determined by the bending of cascade electrons in the magnetic field. The bending angle is estimated as (Tashiro & Vachaspati 2013)

$$\Theta(E_\gamma) \approx 7.3 \times 10^{-5} \left(\frac{B}{10^{-16} \text{G}} \right) \left(\frac{1 \text{Gpc}}{D_s} \right) \left(\frac{E_\gamma}{100 \text{GeV}} \right)^{-3/2}.$$

With $\Theta \approx 12^\circ$, $E_\gamma \approx 10$ GeV, $D_s \approx 1000$ Mpc, we obtain $B \sim 10^{-14}$ G. This value is about two orders of magnitude larger than the lower bound found in Neronov & Vovk (2010) and consistent with the claimed measurement

in Ando & Kusenko (2010) and Essey et al. (2011) (also see Neronov et al. 2011). In this connection we should point out that there is debate on whether pair produced electrons and positrons isotropize due to plasma instabilities (Tavecchio et al. 2010; Dolag et al. 2011; Broderick et al. 2012; Miniati & Elyiv 2013; Schlickeiser et al. 2012) or if their propagation is simply given by bending due to a Lorentz force. Our results favor the latter scenario as it is hard to see how a plasma instability could give rise to a CP violating signature of the type we find.

The energy combinations (E_1, E_2) determine the distance on which the gamma rays probe the magnetic field correlation function. From Eq. (3) with $z_s \sim 1$ and the relation for the observed gamma ray energy, $(E_\gamma/88 \text{ GeV})^{1/2} \sim E_{\text{TeV}}/10 \text{ TeV}$ (Neronov & Semikoz 2009), we find that the (10,40) GeV combination of energies probes distances $\sim 10 \text{ Mpc}$. This should be considered as an order of magnitude estimate since we cannot be sure of the parameters κ and z_s that enter Eq. (3), and also the relation (3) was only derived in the case that the E_3 photon points back to the source.

The results in Fig. 3 show a strong CP violating signal in the (10, 40) GeV panel, less strong signals in the (10, 30) and (20, 40) GeV cases, but not in other energy panels. One possible reason is that we did not detect cascade photons from the same source in all energy bins. Our CP violating signal arises in the energy combination (E_1, E_2, E_3) when cascade photons with energy E_1, E_2 and E_3 come from the same source in the same patch. Since the sources of diffuse gamma rays are unresolved, this suggests that the TeV blazars that source cascade photons are very far and therefore the fluxes of cascade photons are very low. There is a possibility that we have observed cascade photons from the same source in E_1, E_2 and E_3 energy bins but have not yet detected photons in the E'_1 bin. If this is the case, the CP violating signal will be present in the energy combination (E_1, E_2, E_3) but not in (E'_1, E_2, E_3) . Besides, TeV blazars also emit GeV photons directly. Since the photon flux of blazars has a red spectrum, these direct GeV photons from unresolved blazars can dominate cascade photons in diffuse gamma rays. This contamination due to direct GeV photons can reduce the CP violating signals.

The appearance of the CP violation signal only in the (10, 40) GeV panel can also be explained in terms of magnetic field structures. The connection between magnetic field helicity and correlators of gamma ray arrival directions given in Eq. (1) only holds for identified blazars. A more detailed analysis for the diffuse gamma ray flux, though with several simplifying assumptions, shows the correspondence

$$Q = a(E_1, E_2, R)M_H(r_{12}) + a(E_2, E_3, R)M_H(r_{23}) + a(E_3, E_1, R)M_H(r_{31}) \quad (7)$$

where $a(E, E', R)$ is a function of the photon energies and the patch size. Thus the signal seen in a panel depends on the details of the magnetic helicity spectrum at several different length scales, and on combinations of the other parameters. In principle, the signal in the various panels can help us reconstruct the magnetic helicity spectrum, though this will require more detailed investigations, some of which are under way (Tashiro & Vachaspati 2014).

Finally, since we find $Q < 0$, this indicates that the cosmological magnetic field has left-handed helicity. This

could be very interesting for particle physics and early universe cosmology since baryogenesis, which requires fundamental CP violation, predicts magnetic fields with left-handed helicity (Vachaspati 2001), while leptogenesis predicts right-handed helicity (Long et al. 2014). Inflationary models that produce helical magnetic fields have also been proposed (Caprini & Sorbo 2014) and can be distinguished from matter-genesis models by the spectral features of the magnetic fields they produce.

We thank Roger Blandford, Jim Buckley, Nat Butler, Lawrence Krauss, Alexander Kusenko, Owen Littlejohns, Andrew Long and Stefano Profumo for helpful comments. TV is grateful to the IAS, Princeton for hospitality where some of this work was done. We are also grateful for computing resources at the ASU Advanced Computing Center (A2C2). This work was supported by the DOE at ASU and at WU.

REFERENCES

- Ando S., Kusenko A., 2010, *Astrophys.J.*, 722, L39
 Banerjee R., Jedamzik K., 2004, *Phys.Rev.*, D70, 123003
 Boyarsky A., Frohlich J., Ruchayskiy O., 2012, *Phys.Rev.Lett.*, 108, 031301
 Broderick A. E., Chang P., Pfrommer C., 2012, *Astrophys.J.*, 752, 22
 Campanelli L., 2004, *Phys.Rev.*, D70, 083009
 Campanelli L., 2007, *Phys.Rev.Lett.*, 98, 251302
 Caprini C., Durrer R., Kahnashvili T., 2004, *Phys.Rev.*, D69, 063006
 Caprini C., Sorbo L., 2014, [arXiv:1407.2809](https://arxiv.org/abs/1407.2809)
 Christensson M., Hindmarsh M., Brandenburg A., 2005, *Astron.Nachr.*, 326, 393
 Dolag K., Kachelriess M., Ostapchenko S., Tomas R., 2011, *Astrophys.J.*, 727, L4
 Durrer R., Neronov A., 2013, *Astron.Astrophys.Rev.*, 21, 62
 Essey W., Ando S., Kusenko A., 2011, *Astropart.Phys.*, 35, 135
 Kahnashvili T., Ratra B., 2005, *Phys.Rev.*, D71, 103006
 Kahnashvili T., Tevzadze A. G., Brandenburg A., Neronov A., 2013, *Phys.Rev.*, D87, 083007
 Kahnashvili T., Vachaspati T., 2006, *Phys.Rev.*, D73, 063507
 Kunze K. E., 2012, *Phys.Rev.*, D85, 083004
 Long A. J., Sabancilar E., Vachaspati T., 2014, *JCAP*, 02, 036
 Miniati F., Elyiv A., 2013, *Astrophys.J.*, 770, 54
 Neronov A., Semikoz D., 2009, *Phys.Rev.*, D80, 123012
 Neronov A., Semikoz D., Tinyakov P., Tkachev I., 2011, *Astron.Astrophys.*, 526, A90
 Neronov A., Vovk I., 2010, *Science*, 328, 73
 Schlickeiser R., Ibscher D., Supsar M., 2012, *Astro. Phys. J.*, 758, 102
 Tashiro H., Vachaspati T., 2013, *Phys.Rev.*, D87, 123527
 Tashiro H., Vachaspati T., 2014, in progress
 Tavecchio F., Ghisellini G., Foschini L., Bonnoli G., Ghirlanda G., et al., 2010, *Mon.Not.Roy.Astron.Soc.*, 406, L70
 The Fermi-LAT Collaboration, *ApJS* 209, 34A (2013)
 Vachaspati T., 2001, *Phys.Rev.Lett.*, 87, 251302